Magnetoresistance Scaling and the Origin of H-Linear Resistivity in $BaFe_2(As_{1-x}P_x)_2$

Nikola Maksimovic,* Ian M. Hayes, Vikram Nagarajan, and James G. Analytis†
Department of Physics, University of California, Berkeley, California 94720, USA
and Materials Science Division, Lawrence Berkeley National Laboratory,
Berkeley, California 94720, USA

Alexei E. Koshelev
Materials Science Division, Argonne National Laboratory, Lemont, Illinois 60439, USA

John Singleton
National High Magnetic Field Laboratory, Los Alamos National Laboratory,
Los Alamos, New Mexico 87545, USA

Yeonbae Lee and Thomas Schenkel
Materials Science Division, Lawrence Berkeley National Laboratory, Berkeley, California 94720, USA

(Received 2 July 2020; revised 19 October 2020; accepted 23 October 2020; published 29 December 2020)

We explore field and temperature scaling of magnetoresistance in underdoped ($x = 0$, $x = 0.19$) and optimally doped ($x = 0.31$) samples of the high-temperature superconductor $BaFe_2(As_{1-x}P_x)_2$. In all cases, the magnetoresistance is H linear at high fields. We demonstrate that the data can be explained by an orbital model in the presence of strongly anisotropic quasiparticle spectra and scattering time due to antiferromagnetism. In optimally doped samples, the magnetoresistance is controlled by the properties of small regions of the Fermi surface called "hot spots," where antiferromagnetic excitations induce a large quasiparticle scattering rate. The anisotropic scattering rate results in hyperbolic H/T magnetoresistance scaling, which competes with the more conventional Kohler scaling. We argue that these results constitute a coherent picture of magnetotransport in $BaFe_2(As_{1-x}P_x)_2$, which links the origin of H-linear resistivity to antiferromagnetic hot spots. Implications for the T-linear resistivity at zero field are discussed.

DOI: 10.1103/PhysRevX.10.041062 Subject Areas: Condensed Matter Physics

I. INTRODUCTION

The electrical resistivity of certain strange metals has been found to vary linearly with temperature down to low temperature and seems to cross intrinsic energy scales (e.g., the Debye temperature) with impunity; these materials are also characterized by notably rapid quasiparticle scattering [1–5]. It is thought that these phenomena stem from quantum critical physics [6], though an agreed upon explanation of transport in quantum critical metals has still not been established. In recent years, the magnetoresistance (MR) of quantum critical metals has become a subject of intense study, providing another avenue to probe their properties. In particular, in typical metals, the MR varies quadratically with field over an extended field range and is determined by a combination of temperature-dependent and temperature-independent contributions to the resistivity [7]. By contrast, in many quantum critical metals, the MR has been observed to vary linearly with magnetic field over an extended field range [8–17] and to scale only with the temperature-dependent resistivity, suggesting a nontrivial connection between magnetic field (H) and temperature (T) in such materials, but the origin of this behavior is not well understood.

To elucidate the origin of magnetoresistance and scaling, it is useful to partition the resistivity into two contributions—a temperature-independent contribution ρ_0, typically arising from scattering from defects, and a temperature-dependent contribution ρ_t that may arise from charge carrier interactions with phonons, quasiparticle excitations, order parameter fluctuations, and so on. In strange metals, $\rho_t \approx \alpha k_B T$, with α a phenomenological constant of proportionality [1–5].

*nikola_maksimovic@berkeley.edu
†analytis@berkeley.edu

It has been found that a "hyperbolic" magnetoresistance scaling form phenomenologically captures the interplay of field and temperature in strange metals:

$$\frac{\rho(T,H)-\rho_0}{\alpha k_B T} \sim \sqrt{1+\left(\frac{\eta H}{\alpha k_B T}\right)^2}, \tag{1}$$

where $\rho(T,H)$ is the field-dependent resistivity at temperature T and η a parameter that plays a similar role for the field dependence as α does for the temperature dependence [8]. Equation (1) was motivated by measurements of $BaFe_2(As_{1-x}P_x)_2$ near its antiferromagnetic (AFM) quantum critical point. Since then, a growing number of putative quantum critical metals have shown qualitatively similar behavior [8–17], albeit with notable deviations in the quantities α and η. The observation of H-linear magnetoresistance, as suggested by Eq. (1), is unusual but not unprecedented. There are multiple possible causes of H-linear MR, including the presence of Dirac quasiparticles [18,19], sample heterogeneity [20,21], guiding center diffusion in a smooth random potential [22], fluctuations from spin density waves [23,24], or singular regions of the Fermi surface where the Fermi velocity changes discontinuously [7,25]. However, Eq. (1) places further constraints on the origin of the MR, as it conflicts with the conventional Kohler's rule for classical magnetoresistance [7],

$$\frac{\rho(H)-\rho(0)}{\rho(0)} = f\left(\frac{H}{\rho(0)}\right), \tag{2}$$

where f is a smooth and usually positive function. Kohler's rule is satisfied in metals as long as the scattering rate changes uniformly when, for example, the temperature or disorder level is varied. Even if the scattering rate is anisotropic in momentum space, one expects Kohler's rule to be satisfied as long as the "pattern" of anisotropy is unchanged [26]. This constraint of Kohler's scaling is reflected in the denominator of Eq. (2), which takes into account both temperature-independent and temperature-dependent scattering contributions, $\rho(0)=\rho_0+\rho_t$. By contrast, in Eq. (1), the disorder scattering is subtracted, and the quantum critical MR scales only with the T-linear component of the resistivity ($\rho_t=\alpha k_B T$), in apparent violation of Kohler's rule. A realistic theory of magnetotransport in quantum critical metals must simultaneously capture the H-linear MR and the hyperbolic scaling with temperature dictated by Eq. (1). In this paper, we describe such a theory and show that it captures the salient features of experimentally measured MR in $BaFe_2(As_{1-x}P_x)_2$.

Our paper is outlined as follows. First, we describe the theoretical models that we use, which were developed in Refs. [24,25]. These models are based on orbital motion in the presence of anisotropic quasiparticle spectra (turning points) or scattering time (hot spots) due to AFM order and fluctuations, respectively, in $BaFe_2(As_{1-x}P_x)_2$. Second, we demonstrate the validity of the model for the parent compound $BaFe_2As_2$. Third, we explore $BaFe_2(As_{1-x}P_x)_2$ with $x=0.19$ in the antiferromagnetic regime, and discover that the anisotropic scattering rate at this composition leads to a breakdown of Kohler's rule and onset of hyperbolic scaling similar to that described by Eq. (1). Finally, in the quantum critical sample ($x=0.31$), we demonstrate that the model captures the H-linear MR and hyperbolic H/T scaling from first principles. Moreover, we elucidate the role of disorder scattering in Eq. (1) by systematically irradiating samples with alpha particles, and we find that the scaling persists with coefficients that depend on the disorder level, in agreement with the predictions of the hot-spot model. These findings present a coherent picture of magnetotransport in both the antiferromagnetically ordered and quantum critical regimes of $BaFe_2(As_{1-x}P_x)_2$. We comment on possible connections to MR in other iron pnictides and cuprate high-temperature superconductors in the discussion. The implications of these findings for the zero-field T-linear resistivity are left to the discussion.

II. THEORETICAL MODEL

The models for orbital magnetoresistance in the presence of anisotropic quasiparticle spectra or scattering time due to antiferromagnetism were developed in Refs. [24,25]. The Fermi surface of $BaFe_2(As_{1-x}P_x)_2$ is composed of quasicylindrical electron and hole Fermi surfaces with imperfect nesting [27–33]. In the AFM ordered phase ($x<0.31$), the Fermi surface is reconstructed, and a gap opens at points on the Fermi surface nested by the AFM ordering vector due to exchange coupling between conduction electrons and AFM fluctuations. As a quasiparticle undergoes orbital motion in a magnetic field, the Fermi velocity is rapidly reversed at these "turning points" due to the AFM coupling between the electronlike and holelike pockets [25]. This mechanism produces an H^2 variation of the MR at low fields, which crosses over to linear variation at higher fields as the number of quasiparticles pushed through the turning point by the Lorentz force linearly increases with field [7,25]. This contribution coexists with the conventional MR of the rest of the Fermi surface, which is expected to be much smaller than the turning-point MR; we will show that this is consistent with the experimental data, and we will neglect the conventional MR contribution in the present study. Here, we summarize the resulting magnetoresistance from the turning point (see Supplemental Material [34]):

$$\rho^{\mathrm{tp}}(H)-\rho(0) = r_{\mathrm{tp}}\mathcal{B}(H/H_{\mathrm{tp}}), \tag{3}$$

with

$$H_{\mathrm{tp}} = \frac{2c\Delta_{\mathrm{tp}}}{e\tau_{\mathrm{tp}}(v_h v_e \sin\theta_{\mathrm{tp}})} \tag{4}$$

(in CGS units) and

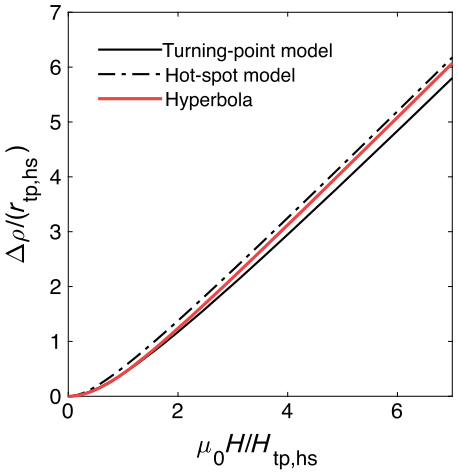

FIG. 1. Hot-spot and turning-point magnetoresistance scaling functions and comparison with hyperbola. The MR $[\Delta\rho = \rho(H) - \rho(H = 0)]$ in both the turning-point and hot-spot models is controlled by two parameters, $r_{\mathrm{tp,hs}}$ and $H_{\mathrm{tp,hs}}$ (tp and hs indicate turning-point and hot-spot, respectively). The derivations of the parameters in terms of antiferromagnetic gap, spin-susceptibility, and electronic-band parameters are given in the Supplemental Material [34]. The MR from the hot spots or turning points follows scaling functions (black lines), with exact expressions given in the Supplemental Material [34]. The functions are well approximated by a hyperbola $\Delta\rho/r_{\mathrm{tp,hs}} = \sqrt{1 + (H/H_{\mathrm{tp,hs}})} - 1$ (red line).

$$r_{\mathrm{tp}} \approx \frac{4(v_{h,x} - v_{e,x})^2 \tau_{\mathrm{tp}} \Delta_{\mathrm{tp}}}{\pi^2 e^2 \hbar^2 \tau_{\mathrm{cold}}^2 s v_h v_e \sin\theta_{\mathrm{tp}} (\frac{n_h}{m_h} + \frac{n_e}{m_e})^2}. \tag{5}$$

Here, Δ_{tp} is the size of the AFM gap, and τ_{tp} and τ_{cold} are the quasiparticle scattering rates in the vicinity of the turning point and in the background; $m_{e,h}$ are effective masses, which are approximately the same for the hole and electron bands [27–31]; $n_{e,h}$ are the band carrier densities; and s is the c-axis lattice parameter. Note that τ_{tp} need not be equal to τ_{cold} because the scattering rate can be anisotropic due to scattering on AFM fluctuations. Here, $\mathbf{v}_{h,e}$ are the Fermi velocities on the hole and electron band, and θ_{tp} is the nesting angle. The dimensionless function $\mathcal{B}(h)$ computed in Ref. [25] has asymptotics $\mathcal{B}(h) \simeq (3\pi/16)h^2$ for $h \ll 1$ and $\mathcal{B}(h) \simeq h$ for $h \gg 1$. This function is plotted in Fig. 1, and its exact shape is presented in the Supplemental Material [34]. Note that this contribution to the MR coexists with the conventional contribution from the rest of the Fermi surface, but it is enhanced by a factor of $\epsilon_f/\Delta_{\mathrm{tp}}$ due to the large curvature at the turning points [25].

When the AFM phase is suppressed to zero temperature by P-substitution [as is the case for $x = 0.31$ $BaFe_2(As_{1-x}P_x)_2$] [35–37], quantum critical spin fluctuations produce strong quasiparticle scattering, and the turning points evolve into hot spots [24,38]. The concept of hot spots was first introduced in the physics of cuprate high-temperature superconductors [39,40]. In a magnetic field, the effect of hot spots on orbital magnetoresistance is similar to that of the turning points [23,24],

$$\rho^{\mathrm{hs}}(H) - \rho(0) = r_{\mathrm{hs}} \mathcal{G}(H/H_{\mathrm{hs}}). \tag{6}$$

The parameters in the hot-spot model, r_{hs} and H_{hs}, are determined by critical spin fluctuations rather than an AFM gap. Both of these parameters scale in the same way with temperature and background scattering time,

$$H_{\mathrm{hs}} = \Gamma_H \frac{T}{\sqrt{\tau_{\mathrm{cold}}}}, \qquad r_{\mathrm{hs}} = \Gamma_r \frac{T}{\sqrt{\tau_{\mathrm{cold}}}}. \tag{7}$$

The coefficients Γ_H and Γ_r depend on the spin-susceptibility and electronic-band parameters (see Supplemental Material [34] for complete expressions), and $\mathcal{G}(h)$ is a dimensionless function with a slightly different exact form compared to the turning-point model in Eq. (3) but qualitatively similar behavior (Fig. 1). Note that, unlike in the turning-point model, the characteristic field scale H_{hs} is determined by the strength of scattering at the hot spot and its region of influence as compared to the background scattering rate, τ_{cold}. Thus, changes to this rate are expected to affect the characteristic field scale in the critical regime.

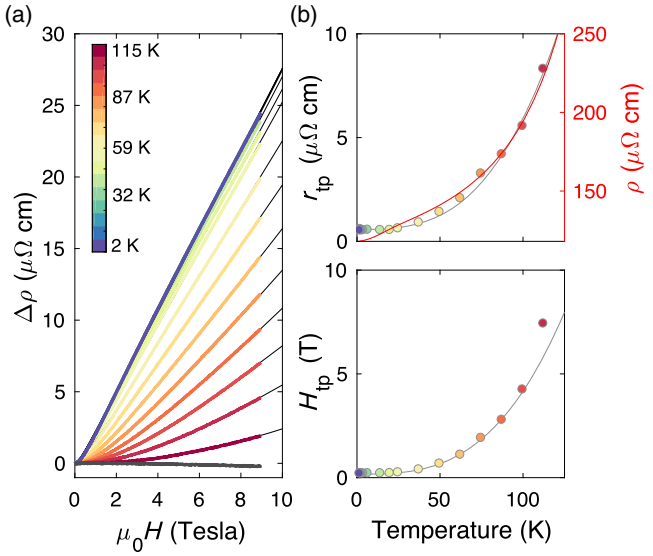

FIG. 2. Transport in $BaFe_2As_2$ and magnetoresistance model based on turning points. (a) Isothermal magnetoresistance at various temperatures. Black lines are fits to the turning-point model given by Eq. (3). (b) Model parameters extracted from the fits; error bars are smaller than the data points. The grey lines show that both parameters vary with T^3 with a finite offset. The red line shows that the zero-field resistivity similarly varies approximately with T^3, suggesting that the MR parameters vary with the scattering rate.

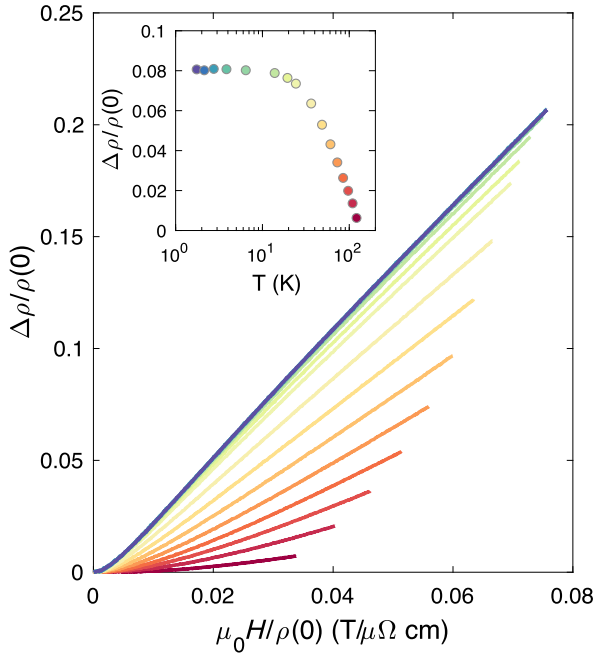

FIG. 3. Kohler's rule in $BaFe_2As_2$. Relative magnetoresistance versus reduced field for different temperatures. The inset shows the temperature dependence of the relative MR at a reduced field of $\mu_0 H/\rho(0) = 0.03$ T/$\mu\Omega$ cm.

Finally, the scaling form of both the turning-point MR [Eq. (9)] and the hot spot MR [Eq. (6)] can be well approximated by a hyperbola (Fig. 1),

$$\mathcal{B}(h),\ \mathcal{G}(h) \approx \sqrt{1+h^2} - 1. \tag{8}$$

This approximation will prove useful when exploring the data in the context of hyperbolic MR scaling and its relation to these models.

III. RESULTS

A. Parent compound $BaFe_2As_2$

The parent compound $BaFe_2As_2$ is nonsuperconducting and has an antiferromagnetic transition at $T_N \approx 135$ K [41]. Its fermiology is well established [27,29,30,32], and previous measurements have reported the H-linear MR in this compound [42]. Here, we explore the MR of an as-grown single crystal in the context of the turning-point model to show that the model accurately simulates the experimentally observed MR.

Figure 2 shows the temperature-dependent MR of $BaFe_2As_2$. The MR is clearly H linear at high fields, consistent with previous observations [42]. We see that the data are well fitted by the turning-point model given by Eq. (3). The two parameters, r_{tp} and H_{tp}, saturate at low temperature and grow with increasing temperature, mimicking the behavior of the resistivity at zero field. This behavior suggests that the changes to the MR coefficients r_{tp} and H_{tp} reflect the temperature-induced enhancement of the scattering rate in agreement with Eqs. (4) and (5). At low temperature, both MR parameters saturate, suggesting a single dominant scattering rate that is independent of temperature, likely due to disorder. Indeed, in Fig. 3, we observe that the MR amplitude saturates below 10 K. The failure of Kohler's rule as temperature increases can be attributed to temperature-induced anisotropic scattering due to spin waves

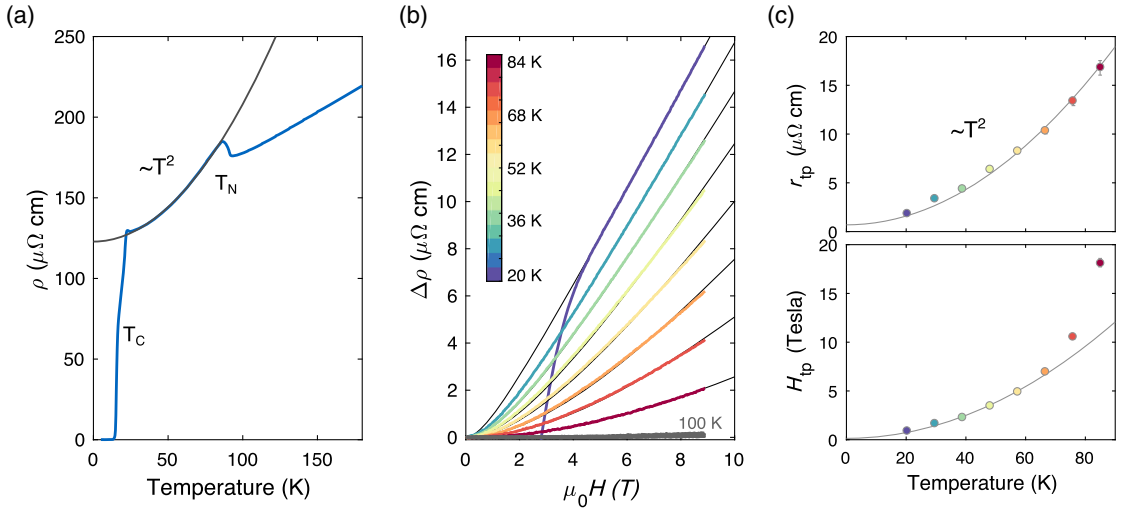

FIG. 4. Transport in $BaFe_2(As_{0.81}P_{0.19})_2$ and magnetoresistance model based on turning points. (a) Resistivity shows a transition to an AFM ordered state ($T_N \approx 95$ K), and superconducting state beginning at $T_c = 22$ K with zero resistance at 15 K. Inside the AFM state, the resistivity varies with T^2, with a finite $T = 0$ intercept. The data are fitted well by $\rho(H = 0) = 122.8\ [\mu\Omega\,\mathrm{cm}] + 0.0085\ [\mu\Omega\,\mathrm{cm/K^2}] \times T^2$ (black line). (b) Magnetoresistance for different temperatures with fits to the turning-point MR model [Eq. (3)] indicated by black lines. (c) Fit parameters of the model plotted as a function of temperature, with a best-fit line to the data below 70 K. Here, $H_{tp} = 0.098[\mathrm{T}] + 0.0015\ [\mathrm{T/K^2}] \times T^2$, and $r_{tp} = 0.69\ [\mu\Omega\,\mathrm{cm}] + 0.0023\ [\mu\Omega\,\mathrm{cm/K^2}] \times T^2$.

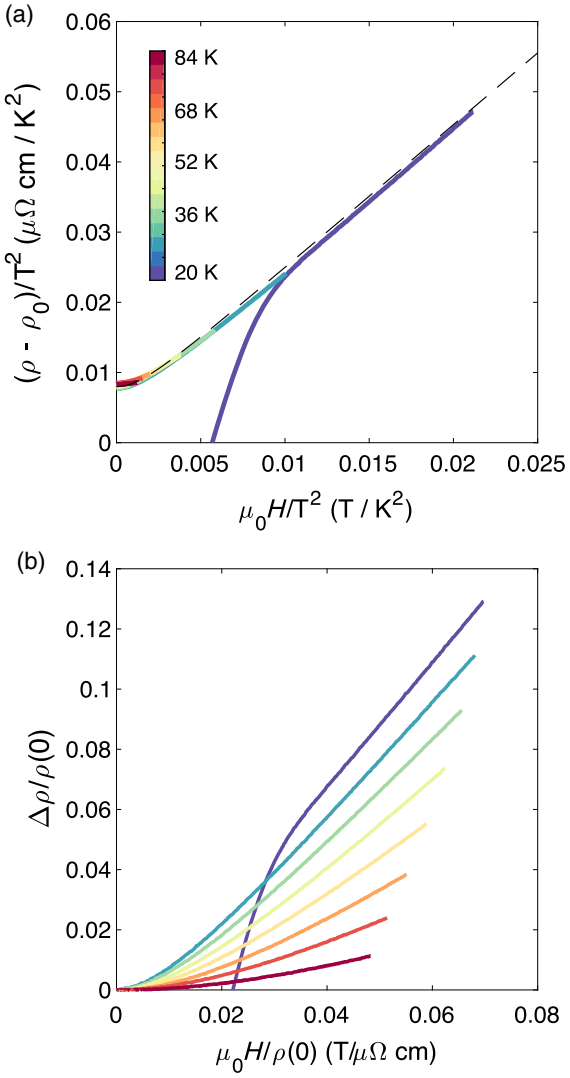

FIG. 5. Comparison of hyperbolic magnetoresistance scaling and Kohler's rule inside the AFM ordered state of $BaFe_2(As_{0.81}P_{0.19})_2$. (a) A simple hyperbolic scaling relation holds, where the residual resistivity $\rho_0 = 122\ \mu\Omega\,\mathrm{cm}$ is first subtracted. The dashed black line is the expression given by Eq. (9) with $\beta = 0.0039\ [\mu\Omega\,\mathrm{cm/K^2}]$, $\alpha' = 0.0085\ [\mu\Omega\,\mathrm{cm/K^2}]$, and $\gamma = 0.0015\ [\mathrm{T/K^2}]$. (b) Kohler's rule is violated as a function of temperature.

[43] in combination with a potentially temperature-dependent AFM gap.

The dominant role of isotropic disorder scattering at low temperature allows us to evaluate the plausibility of the model parameters. Using the known values of carrier density and effective mass ($n_e = 1.17 \times 10^{20}\ \mathrm{cm^{-3}}$, $n_h = 1.23 \times 10^{20}\ \mathrm{cm^{-3}}$, and $m \approx 2m_e$ for both electrons and holes) [27], the Drude estimate of the residual scattering time is $\tau = \tau_{\mathrm{cold}} = \tau_{\mathrm{tp}} = 3 \times 10^{-13}$ s ($\rho_0 \approx 100\ \mu\Omega\,\mathrm{cm}$). The previously quoted values of Fermi velocity vary between 0.5×10^7 cm/s and 2.5×10^7 cm/s [30,32,44]. With the Drude scattering time above, Eq. (4) gives an AFM gap of $\Delta \approx 1$ meV using the low-temperature $H_{\mathrm{tp}} \approx 0.2$ T and a Fermi velocity of $v_F \approx 2 \times 10^7$ cm/s [44]. This result is considerably lower than the AFM gap $\Delta \approx 10$ meV expected for the transition temperature of 135 K, but it is at least consistent within an order of magnitude. Better agreement is found if the relevant scattering time is in fact lower than the Drude estimate ($\sim 10^{-12}$ s), which is a possibility considering that the Drude estimate may be inaccurate for this multiband system. Alternatively, there may be a deeper reason for the relatively small effective gap at the turning point. Parity constraints cause the hybridization between hole and electron bands to vanish at $k_x = 0$ [33]; because the turning points are close to this axis, this process could result in a suppression of the effective AFM gap near the turning point.

On a final note, while approximately H-linear MR can exist over a narrow range of field in compensated metals such as $BaFe_2As_2$ [7], this is only expected to occur close to the high-field limit when $\omega_c\tau = eH\tau/mc \approx 1$. From the above considerations, we estimate that $\omega_c\tau = 1$ at 40 T in this sample. The experimental MR therefore becomes H linear well below the conventional high-field limit.

B. Underdoped $BaFe_2(As_{1-x}P_x)_2$ with $x = 0.19$

Here, we examine a single crystal of $BaFe_2(As_{1-x}P_x)_2$ with $x = 0.19$, where the antiferromagnetic Néel transition temperature is $T_N \approx 95$ K. In Fig. 4, transport data are shown for this crystal. Figure 4(a) shows that the resistivity at zero applied field varies with T^2 over a broad range of temperature inside the AFM ordered state with a finite intercept at $T = 0$. At this composition, the resistivity is likely influenced by anisotropic quasiparticle scattering from diffuse spin fluctuations [43,45].

Figure 4(b) shows the MR inside the AFM state, which displays H-linear behavior at high fields. Note that the measured relative MR just below T_N is a factor of 12 larger than the MR just above T_N, suggesting that the turning points again provide a dominant contribution to the measured MR. We therefore neglect the conventional MR contribution when modeling the data. The data are well fitted by the turning-point model given by Eq. (3), with the temperature-dependent parameters shown in Fig. 4(c). Again, the MR parameters follow a similar temperature dependence to that of the zero-field resistivity, suggesting the MR parameters vary with the scattering time. The amplitude of the MR and characteristic field are slightly different in this composition than in $BaFe_2As_2$. This difference can likely be attributed to changes in the AFM gap or scattering time induced by P-substitution. Unfortunately, the fermiology is not well established at this composition, but assuming comparable parameters to the parent compound, these measurements are in the low-field limit of orbital MR (i.e., $\omega_c\tau \ll 1$).

We find that a hyperbolic MR scaling can be derived from our model at this composition. From Fig. 4(c), we observe that the offsets of $H_{\mathrm{tp}} = \gamma T^2 + \gamma_0$ and $r_{\mathrm{tp}} = \beta T^2 + \beta_0$ are relatively small compared to the temperature

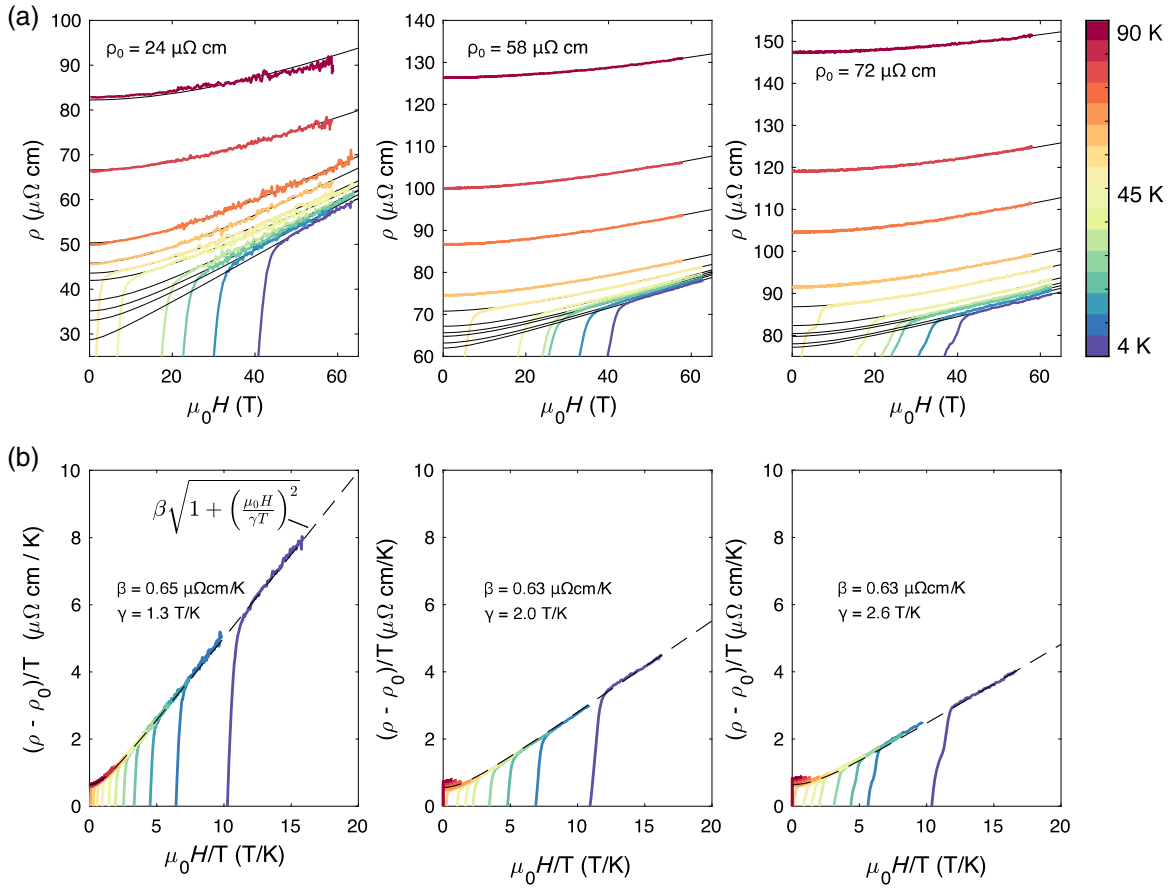

FIG. 6. Magnetoresistance, hot-spot model, and hyperbolic scaling in $BaFe_2(As_{0.81}P_{0.31})_2$ with varying levels of disorder. (a) Samples showing clear H-linear dependence at high fields. Black lines are fits to the hot-spot MR model given by Eq. (6). Each panel is labeled by the extrapolated zero-temperature resistivity, which quantifies the level of disorder. (b) Hyperbolic scaling of MR for each respective sample. Dashed lines are hyperbolic functions with the parameters shown in each figure.

dependence over the measured range and can be neglected (at the lowest measured temperature 20 K, $\beta_0/\beta T^2 \approx 0.3$, and $\gamma_0/\gamma T^2 \approx 0.1$). Plugging in $\rho(0) = \rho_0 + \alpha' T^2$, $H_{\rm tp} \approx \gamma T^2$, and $r_{\rm tp} \approx \beta T^2$ into a hyperbolic approximation of the turning-point MR [Eq. (8)], we obtain

$$\frac{\rho(H) - \rho_0}{T^2} \approx \beta \sqrt{1 + \left(\frac{\mu_0 H}{\gamma T^2}\right)^2} + \alpha' - \beta. \qquad (9)$$

The applicability of this hyperbolic scaling relation to the MR of the $x = 0.19$ sample is shown in Fig. 5(a). By contrast, conventional Kohler scaling fails, as shown in Fig. 5(b). The MR scales only with the temperature-dependent scattering rate despite the rather large residual resistivity. The scaling shown in Fig. 5(a) is similar to the established phenomenology [Eq. (1)] for the MR of quantum critical metals in the literature—the difference is that this is realized in the AFM ordered state rather than the quantum critical regime, and the temperature-dependent resistivity varies with T^2 rather than with T. This difference is reflected in the different temperature dependence of the denominator in Eq. (9) compared to Eq. (1).

The validity of hyperbolic scaling described by Eq. (9) and the failure of Kohler's rule are rooted in the apparent anisotropy of the scattering rate. In particular, the MR parameters are controlled by the scattering rate at the turning points, and the small offsets of $r_{\rm tp}(T)$ and $H_{\rm tp}(T)$ indicate that the temperature-dependent scattering rate at the turning point is much larger than the temperature-independent residual contribution over the measured range. Thus, the MR is primarily controlled by the temperature dependence independently of the residual resistivity. Quantitatively, we estimate that the inelastic T^2 scattering near the turning point is enhanced by a factor of $[\beta T^2/\beta_0]/[\alpha' T^2/\rho_0] \approx 100$ over the background scattering rate; this result is in contrast with the relatively small changes in the overall resistivity $\rho(20K)/\rho_0 \approx 1.03$, which averages the scattering rate over the whole Fermi surface. The presence of multiple scattering times, one of which is anisotropic, explains the violation of Kohler's rule observed in Fig. 5(b) [26]. It is not surprising that the scattering rate at the turning point is much higher than the background,

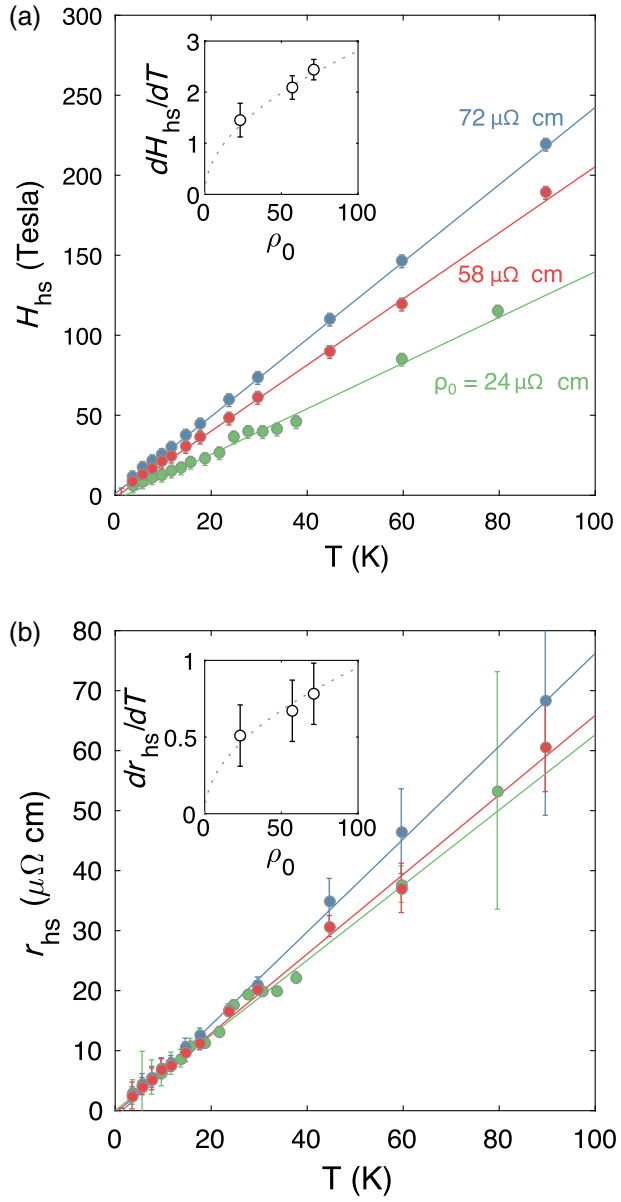

FIG. 7. Hot-spot parameters in $BaFe_2(As_{1-x}P_x)_2$ with $x = 0.31$. (a) Characteristic field H_{hs} as a function of temperature with a linear fit for each sample. The inset shows the slope of $H_{hs}(T)$ versus the residual resistivity. The dotted line shows the expected $\rho_0^{1/2}$ dependence according to Eq. (7) of the hot-spot model. (b) Hot-spot MR amplitude. The inset shows the slope of $r_{hs}(T)$ versus the residual resistivity with a fit to the expected $\rho_0^{1/2}$ dependence. Error bars are derived from the confidence intervals of the hot-spot fits and the linear fits in the present figure.

given the presence of diffuse spin fluctuations centered at turning points in underdoped $BaFe_2As_2$ [43]. This result implies that the turning point is simultaneously a hot spot, where the turning-point MR dominates as long as the region of hot-spot scattering is much larger than the width of the turning point. At sufficiently low temperature, spin fluctuations should be damped, and the isotropic disorder scattering contribution becomes dominant. We expect the hyperbolic scaling shown in Fig. 5 to fail and for Kohler's rule to be restored when $\beta_0/\beta T^2 < 1$ (i.e., at T < 10 K). Unfortunately, the superconducting critical field at this composition makes this temperature regime inaccessible in our measurement apparatus.

C. Quantum critical $BaFe_2(As_{1-x}P_x)_2$ with $x = 0.31$

In this sample, the AFM phase is suppressed to zero temperature, and the turning points evolve into hot spots characterized by scattering from critical spin fluctuations [24,35–37]. The phenomenological H/T scaling given by Eq. (1) is known to describe the MR of this composition [8]. Here, we show that this behavior can be captured by the hot-spot MR model given by Eq. (6), as the characteristic parameters are predicted to have a linear variation with temperature. Moreover, as discussed in the theory section, an effective experimental method to test this model in the quantum critical regime is to vary the background scattering rate (τ_{cold}), for example, by varying the concentration of defects in the underlying crystal lattice. This method is expected to alter the characteristic field scale determining the crossover between H^2 and H-linear MR [Eq. (7)]. We accomplish this experimentally with 3-MeV alpha-particle irradiation of samples with $x = 0.31$ phosphorous substitution. This irradiation method produces isotropic defects with a distribution of radii (from pointlike to nm in radius) [46], which increase the residual resistivity at zero field and temperature. The temperature-dependent resistivity follows a T-linear dependence, which is not significantly affected by irradiation (see Supplemental Material [34]).

Figure 6(a) shows the magnetoresistance for samples in the quantum critical regime with varying concentration of defects. The MR data for each sample across a range of temperatures can be well fitted by Eqs. (6) and (7). Figure 6(b) shows that each sample obeys the hyperbolic H/T scaling form described in the Introduction; this scaling is not qualitatively affected by a factor of 3 increase in the residual resistivity, but there is a notable change in the coefficients of the scaling function.

Here, we show that H/T MR scaling and the disorder dependence of the coefficients are captured by our hot-spot MR model. As shown in Fig. 7, the hot-spot parameters extracted from the fits have the following temperature dependence: $H_{hs} \approx \gamma T$ and $r_{hs} \approx \beta T$, consistent with the theory predictions [Eq. (7)]. We note that the offsets of r_{hs} and H_{hs} are essentially zero within the error bars and can be neglected. Using the hyperbolic approximation of the hot-spot MR scaling function, Eq. (8), along with $H_{hs} = \gamma T$, $r_{hs} = \beta T$, and $\rho = \rho_0 + \alpha T$, we arrive at the hyperbolic H/T scaling relation

$$\frac{\rho(H) - \rho_0}{T} \approx \beta \sqrt{1 + \left(\frac{\mu_0 H}{\gamma T}\right)^2} - \beta + \alpha. \qquad (10)$$

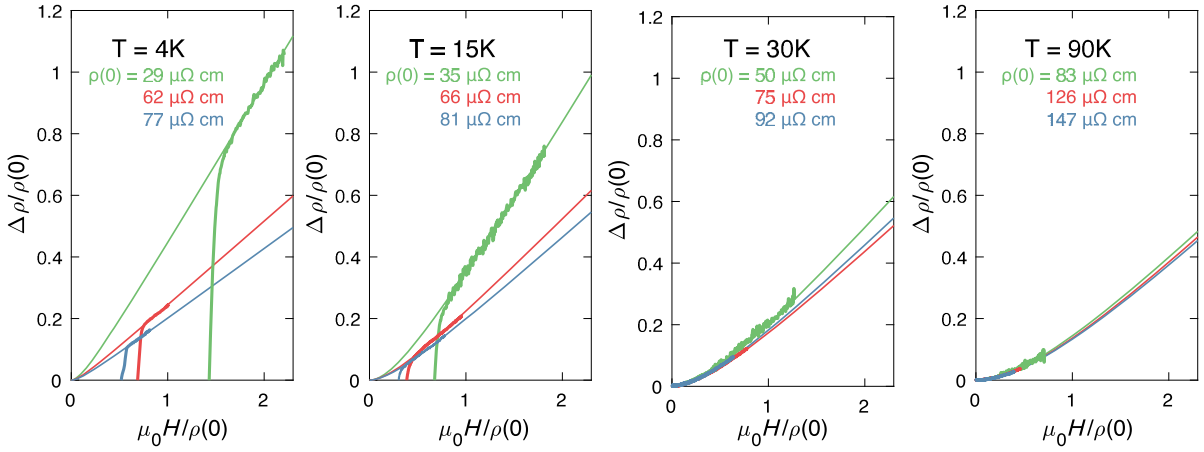

FIG. 8. Isothermal Kohler's rule in quantum critical $BaFe_2(As_{1-x}P_x)_2$ ($x = 0.31$). A comparison of the isothermal magnetoresistance of separate samples with varying doses of alpha-particle irradiation. The violation of Kohler's rule in the linear MR regime suggests that disorder scattering alters the degree of scattering anisotropy, in agreement with the hot-spot model. Solid lines are fits to Eq. (6), for which the zero-field resistivity is extracted from each trace. The curves are labeled by the resistivity of the sample at zero field at the given temperature. Note that $\mu_0 H/\rho(0)$ is in units of Tesla/$\mu\Omega$ cm.

Figure 6(b) shows the validity of this hyperbolic scaling relation. Note that Eq. (10) has a form similar to the phenomenological scaling established by Eq. (1). We emphasize that this scaling results from the T-linear dependence of hot-spot parameters, which is a direct prediction of our MR model [Eq. (7)]. In addition, the small offset of $r_{\rm hs}$ manifests the dominant role of inelastic scattering over background disorder scattering at the hot spot over the measured range; this case is similar to the situation at $x = 0.19$ and is an essential property for realizing the hyperbolic MR scaling.

Figure 7 shows the T-linear dependence of the hot-spot parameters extracted from the experimental data in agreement with Eq. (7) of the theory. Notably, Fig. 7(a) shows that the characteristic field scale $H_{\rm hs}$ increases as the background scattering rate increases. The square-root dependence of this field scale on the disorder scattering rate is consistent with the expectation of the hot-spot model [Eq. (7), where $\rho_0 \sim \tau_{\rm cold}^{-1}$]. This dependence is reflected in the broadening of the hyperbolic MR as the disorder level increases, as shown in Fig. 6(b). We also observe that the gradient of $r_{\rm hs}(T)$ increases as the disorder level increases, in agreement with Eq. (7), though the error bars from the fits are comparably larger for this parameter.

We also perform tests of Kohler's rule at fixed temperature, where the scattering rate is varied by disorder to further verify the hot-spot model. In Fig. 8, we show that at a fixed temperature in $BaFe_2(As_{1-x}P_x)_2$ ($x = 0.31$), Kohler's rule is violated in the high-field linear magnetoresistance regime, but it is satisfied in the low-field quadratic regime. The failure of Kohler's rule in the linear magnetoresistance regime at a fixed temperature reflects the fact that the background disorder scattering alters the pattern of scattering anisotropy as predicted by our hot-spot model in Eq. (7) and the text surrounding it. This result is also consistent with the nontrivial dependence of the characteristic field $H_{\rm hs}$ on disorder [Fig. 7(a)]. The validity of Kohler's rule in the low-field quadratic regime confirms the orbital origin of the MR in the quantum critical composition of $BaFe_2(As_{1-x}P_x)_2$. In the low-field limit, the majority of quasiparticles have not yet been pushed into the hot spot (a conservative estimate of $\omega_c\tau = 1$ is 100 Tesla), so only a small fraction of a cyclotron orbit has been completed.

IV. DISCUSSION

The H-linear MR of $BaFe_2(As_{1-x}P_x)_2$ can be reconciled as an orbital response with a highly anisotropic structure in the Fermi surface—either due to the presence of a gap or a hot spot—at points on the Fermi surface nested by the antiferromagnetic ordering vector. In the critical regime, spin fluctuations result in a linear increase of the hot-spot scattering with temperature, which underlies the hyperbolic H/T scaling of MR at $x = 0.31$ [8]. Another important ingredient for realizing hyperbolic MR scaling is that the disorder scattering rate at the hot spot is comparably smaller than the inelastic spin-fluctuation scattering rate, and therefore, the MR is primarily controlled by the temperature-dependent resistivity. This interpretation is confirmed by our observation of hyperbolic H/T^2 scaling in $BaFe_2(As_{1-x}P_x)_2$ with $x = 0.19$ in the AFM regime. Note that this case does not imply that ρ_0 is small compared to ρ_t, only that the effect of disorder on the hot-spot scattering rate is small compared to its temperature dependence. Consequently, hyperbolic scaling is expected to break down and give way to Kohler scaling at the lowest temperature where disorder scattering becomes dominant. We indeed observe a weak deviation

from hyperbolic scaling in the most disordered $x = 0.31$ sample at 1.5 K (see Supplemental Material [34]). Experiments at lower temperatures and sufficiently high magnetic fields to destroy superconductivity are necessary to explore the potential restoration of Kohler scaling in the low-temperature limit.

Our study shows that the temperature dependence of the hot-spot or turning-point parameters is strongly influenced by the P-substitution level [Figs. 2(b), 4(c), and 7]. For example, the temperature scaling of the characteristic field goes from T^3 to T^2 to T linear, following a similar trend as the zero-field resistivity, as the P concentration tunes the system towards the critical point at $x = 0.31$. This process may reflect the character of spin-excitation scattering and AFM gap as a function of P-substitution. In particular, neutron scattering experiments show that the well-defined spin waves of $BaFe_2As_2$ become increasingly diffusive spin fluctuations as the material is doped [43]. It is likely that diffusive spin fluctuations result in a relatively high scattering rate at the hot spots or turning points at $x = 0.19$ and $x = 0.31$, which contributes to the onset of hyperbolic scaling at those compositions. This case is in contrast to the parent compound $BaFe_2As_2$ where the spin waves are sharply defined [43], and the hyperbolic scaling fails (see Supplemental Material [34]). Notably, it is thought that the diffusive spin fluctuations at moderate doping levels also provide a pairing mechanism for superconductivity [43,47], and therefore, it would be interesting to explore the possible correlation between hyperbolic MR scaling and superconductivity in $BaFe_2(As_{1-x}P_x)_2$ [9]. The present study shows that MR measurements may be useful for probing hot-spot properties across the P-substituted phase diagram, potentially providing valuable quantitative information as to how spin excitations influence the resistivity, and ultimately superconductivity, in iron-based superconductors [47]. Note that compositions of $BaFe_2(As_{1-x}P_x)_2$ also undergo a tetragonal-to-orthorhombic distortion when cooling through T_N. The resulting twin boundaries in single crystals are expected to induce temperature-independent scattering, which can be parametrized by the disorder scattering rate in our model.

The proximity to a nematic quantum critical point [48] suggests nematic fluctuations could also affect the resistivity [47,49–52]. However, our model naturally captures the MR over a wide range of the phase diagram, and therefore, it seems that the influence of nematic order on the MR can be neglected in this material. On the other hand, $FeSe_{1-x}S_x$ near a putative nematic QCP [53] shows very similar MR to that of $BaFe_2(As_{1-x}P_x)_2$ [11]. It is possible that the nearby magnetism in $FeSe_{1-x}S_x$ has a strong influence on the MR, and the present hot-spot model is applicable to that material [54,55]. Another option is that nematic fluctuations effectively create hot spots in $FeSe_{1-x}S_x$ [49], but the differences between $BaFe_2(As_{1-x}P_x)_2$ and $FeSe_{1-x}S_x$ should be explored further. Note that while the conventional MR contribution of our samples can be neglected due to the high level of disorder scattering, a coexistence of conventional orbital MR with a quantum critical component has been observed in very clean samples of $Fe(Se_{1-x}S_x)$ [11]. In the language of the present study, this case can be interpreted as a parallel contribution of orbital MR from the cold and hot spots, where the latter induces a hyperbolic dependence of the MR on H.

Given that the hot-spot model accurately captures the MR of $BaFe_2(As_{1-x}P_x)_2$ and the H/T scaling, it is likely that the AFM fluctuations are the source of the anomalous T-linear resistivity in the quantum critical regime. However, while the hot-spot regions are expected to give a correction to the conductivity that is linear in T (see Supplemental Material [34]), at zero field, the cold parts of the Fermi surface are expected to dominate [39]. Within a nearly antiferromagnetic Fermi-liquid framework, one option is that mixing of hot-spot and disorder scattering leads to nontrivial behavior of the overall resistivity [23,56]. Our data are difficult to reconcile with such a mechanism for temperatures above T_c—disorder adds a temperature-independent component to the resistivity consistent with Matthiessen's rule, which can only occur if the temperature-dependent scattering is independent of disorder. Other nearly antiferromagnetic Fermi-liquid models show that magnetic fluctuations at hot spots can influence the overall resistivity through multiple scattering [57], or the so-called backflow effect [58]. A more recent revival of the hot-spot picture has shown that an unconventional two-particle scattering process connecting hot and cold regions can render the entire Fermi surface a "marginal" Fermi liquid with an overall T-linear resistivity [59]. A theory of orbital MR in a marginal Fermi liquid would be an interesting extension of the present study.

Finally, hot spots at the antinodal regions of the Brillouin zone of the cuprates have been suggested as a source of anomalous behavior in transport and photoemission measurements for some time [60,61], so in light of our results, the recent observations of H-linear magnetoresistance in both electron- and hole-doped cuprate superconductors may be interpreted as a result of antiferromagnetic fluctuations at hot spots [9,17]. This picture of an anisotropic scattering rate would also explain a long-standing question regarding the violation of Kohler's rule observed in the cuprates [62]. Moreover, scaling behavior with the cotangent of the Hall angle has been observed in many quantum critical metals, the so-called "modified" Kohler's rule [63,64], and we leave the question of whether this can be captured in the present hot-spot model to future work.

ACKNOWLEDGMENTS

We thank F. F. Balakirev and R. McDonald for their support during pulsed-field experiments. We also thank R. McDonald, A. Patel, E. Altman, E. Berg, R. Fernandez,

D. Maslov, and N. E. Hussey for valuable discussions and insights. Experimental data on pristine $BaFe_2(As_{1-x}P_x)_2$ ($x = 0.31$) were previously published in Ref. [8] and reprinted here with permission. This work was supported as part of the Center for Novel Pathways to Quantum Coherence in Materials, an Energy Frontier Research Center funded by the U.S. Department of Energy, Office of Science. N. M. was supported by the Gordon and Betty Moore Foundations EPiQS Initiative through Grant No. GBMF 9067. The work of A. E. K. in Argonne was supported by the U.S. Department of Energy, Office of Science, Basic Energy Sciences, Materials Sciences and Engineering Division. A portion of this work was performed at the National High Magnetic Field Laboratory, which is supported by the National Science Foundation Cooperative Agreement No. DMR-1157490 and the State of Florida.

N. M. fabricated the devices and carried out the low-field measurements. N. M., Y. L., and T. S. carried out sample irradiation. N. M., V. N., I. M. H., and J. S. carried out the pulsed-field experiments. N. M. and A. E. K. performed the theoretical modeling. N. M. and I. M. H. grew the crystals. All authors contributed to writing the manuscript.

[1] A. Legros, S. Benhabib, W. Tabis, F. Laliberté, M. Dion, M. Lizaire, B. Vignolle, D. Vignolles, H. Raffy, Z. Z. Li, P. Auban-Senzier, N. Doiron-Leyraud, P. Fournier, D. Colson, L. Taillefer, and C. Proust, *Universal T-Linear Resistivity and Planckian Dissipation in Overdoped Cuprates*, Nat. Phys. **15**, 142 (2019).

[2] J. A. N. Bruin, H. Sakai, R. S. Perry, and A. P. Mackenzie, *Similarity of Scattering Rates in Metals Showing T-Linear Resistivity*, Science **339**, 804 (2013).

[3] H. v. Löhneysen, T. Pietrus, G. Portisch, H. G. Schlager, A. Schröder, M. Sieck, and T. Trappmann, *Non-Fermi-Liquid Behavior in a Heavy-Fermion Alloy at a Magnetic Instability*, Phys. Rev. Lett. **72**, 3262 (1994).

[4] P. Fournier, P. Mohanty, E. Maiser, S. Darzens, T. Venkatesan, C. J. Lobb, G. Czjzek, R. A. Webb, and R. L. Greene, *Insulator-Metal Crossover near Optimal Doping in* $Pr_{2x}Ce_xCuO_4$*: Anomalous Normal-State Low Temperature Resistivity*, Phys. Rev. Lett. **81**, 4720 (1998).

[5] S. A. Grigera, R. S. Perry, A. J. Schofield, M. Chiao, S. R. Julian, G. G. Lonzarich, S. I. Ikeda, Y. Maeno, A. J. Millis, and A. P. Mackenzie, *Magnetic Field-Tuned Quantum Criticality in the Metallic Ruthenate* $Sr_3Ru_2O_7$, Science **294**, 329 (2001).

[6] P. Coleman and A. J. Schofield, *Quantum Criticality*, Nature (London) **433**, 226 (2005).

[7] A. B. Pippard, *Magnetoresistance in Metals* (Cambridge University Press, Cambridge, England, 1989).

[8] I. M. Hayes, R. D. McDonald, N. P. Breznay, T. Helm, P. J. W. Moll, M. Wartenbe, A. Shekhter, and J. G. Analytis, *Scaling between Magnetic Field and Temperature in the High-Temperature Superconductor* $BaFe_2(As_{1-x}P_x)_2$, Nat. Phys. **12**, 916 (2016).

[9] T. Sarkar, P. R. Mandal, N. R. Poniatowski, M. K. Chan, and R. L. Greene, *Correlation between Scale-Invariant Normal-State Resistivity and Superconductivity in an Electron-Doped Cuprate*, Sci. Adv. **5**, eaav6753 (2019).

[10] R. Prozorov, M. Kończykowski, M. A. Tanatar, A. Thaler, S. L. Bud'ko, P. C. Canfield, V. Mishra, and P. J. Hirschfeld, *Effect of Electron Irradiation on Superconductivity in Single Crystals of* $Ba(Fe_{1-x}Ru_x)_2As_2$ *($x = 0.24$)*, Phys. Rev. X **4**, 041032 (2014).

[11] S. Licciardello, N. Maksimovic, J. Ayres, J. Buhot, M. Čulo, B. Bryant, S. Kasahara, Y. Matsuda, T. Shibauchi, V. Nagarajan, J. G. Analytis, and N. E. Hussey, *Coexistence of Orbital and Quantum Critical Magnetoresistance in* $FeSe_{1-x}S_x$, Phys. Rev. Research **1**, 023011 (2019).

[12] Q. Niu, W. C. Yu, K. Y. Yip, Z. L. Lim, H. Kotegawa, E. Matsuoka, H. Sugawara, H. Tou, Y. Yanase, and S. K. Goh, *Quasilinear Quantum Magnetoresistance in Pressure-Induced Nonsymmorphic Superconductor Chromium Arsenide*, Nat. Commun. **8**, 15358 (2017).

[13] Y. Nakajima, T. Metz, C. Eckberg, K. Kirshenbaum, A. Hughes, R. Wang, L. Wang, S. R. Saha, I.-L. Liu, N. P. Butch, D. Campbell, Y. S. Eo, D. Graf, Z. Liu, S. V. Borisenko, P. Y. Zavalij, and J. Paglione, *Quantum-Critical Scale Invariance in a Transition Metal Alloy*, Commun. Phys. **3**, 181 (2020).

[14] B. C. Sales, K. Jin, H. Bei, G. M. Stocks, G. D. Samolyuk, A. F. May, and M. A. McGuire, *Quantum Critical Behavior in a Concentrated Ternary Solid Solution*, Sci. Rep. **6**, 26179 (2016).

[15] J.-H. Chu, J. Liu, H. Zhang, K. Noordhoek, S. C. Riggs, M. Shapiro, C. R. Serro, D. Yi, M. Mellisa, S. J. Suresha, C. Frontera, E. Arenholz, A. Vishwanath, X. Marti, I. R. Fisher, and R. Ramesh, *Possible Scale Invariant Linear Magnetoresistance in Pyrochlore Iridates* $Bi_2Ir_2O_7$, New J. Phys. **21**, 113041 (2019).

[16] R. Kumar, S. Singh, and S. Nair, *High Temperature Linear Magnetoresistance and Scaling Behavior in the* $Ba(Fe_{1-x}Co_x)_2As_2$ *Series*, arXiv:1801.03768v1.

[17] P. Giraldo-Gallo, J. A. Galvis, Z. Stegen, K. A. Modic, F. F. Balakirev, J. B. Betts, X. Lian, C. Moir, S. C. Riggs, J. Wu, A. T. Bollinger, X. He, I. Božović, B. J. Ramshaw, R. D. McDonald, G. S. Boebinger, and A. Shekhter, *Scale-Invariant Magnetoresistance in a Cuprate Superconductor.*, Science **361**, 479 (2018).

[18] A. A. Abrikosov, *Quantum Linear Magnetoresistance*, Europhys. Lett. **49**, 789 (2000).

[19] H. K. Pal and D. L. Maslov, *Linear Magnetoresistance from Dirac-like Fermions in Graphite*, Phys. Rev. B **88**, 035403 (2013).

[20] P. Majumdar and P. B. Littlewood, *Dependence of Magnetoresistivity on Charge-Carrier Density in Metallic Ferromagnets and Doped Magnetic Semiconductors*, Nature (London) **395**, 479 (1998).

[21] N. Ramakrishnan, Y. T. Lai, S. Lara, M. M. Parish, and S. Adam, *Equivalence of Effective Medium and Random Resistor Network Models for Disorder-Induced Unsaturating Linear Magnetoresistance*, Phys. Rev. B **96**, 224203 (2017).

[22] J. C. W. Song, G. Refael, and P. A. Lee, *Linear Magnetoresistance in Metals: Guiding Center Diffusion in a Smooth Random Potential*, Phys. Rev. B **92**, 180204(R) (2015).

[23] A. Rosch, *Magnetotransport in Nearly Antiferromagnetic Metals*, Phys. Rev. B **62**, 4945 (2000).

[24] A. E. Koshelev, *Magnetotransport of Multiple-Band Nearly Antiferromagnetic Metals Due to Hot-Spot Scattering*, Phys. Rev. B **94**, 125154 (2016).

[25] A. E. Koshelev, *Linear Magnetoconductivity in Multiband Spin-Density-Wave Metals with Nonideal Nesting*, Phys. Rev. B **88**, 060412(R) (2013).

[26] R. S. Sorbello, *Effects of Anisotropic Scattering on Electronic Transport Properties*, Phys. Condens. Matter **19**, 303 (1975).

[27] T. Terashima, N. Kurita, M. Tomita, K. Kihou, C. H. Lee, Y. Tomioka, T. Ito, A. Iyo, H. Eisaki, T. Liang, M. Nakajima, S. Ishida, S. I. Uchida, H. Harima, and S. Uji, *Complete Fermi Surface in* $BaFe_2As_2$ *Observed via Shubnikov–de Haas Oscillation Measurements on Detwinned Single Crystals*, Phys. Rev. Lett. **107**, 176402 (2011).

[28] H. Shishido, A. F. Bangura, A. I. Coldea, S. Tonegawa, K. Hashimoto, S. Kasahara, P. M. C. Rourke, H. Ikeda, T. Terashima, R. Settai, Y. Onuki, D. Vignolles, C. Proust, B. Vignolle, A. McCollam, Y. Matsuda, T. Shibauchi, and A. Carrington, *Evolution of the Fermi Surface of* $BaFe_2(As_{1-x}P_x)_2$ *on Entering the Superconducting Dome*, Phys. Rev. Lett. **104**, 057008 (2010).

[29] M. F. Jensen, V. Brouet, E. Papalazarou, A. Nicolaou, A. Taleb-Ibrahimi, P. Le Fèvre, F. Bertran, A. Forget, and D. Colson, *Angle-Resolved Photoemission Study of the Role of Nesting and Orbital Orderings in the Antiferromagnetic Phase of* $BaFe_2As_2$, Phys. Rev. B **84**, 014509 (2011).

[30] J. Fink, S. Thirupathaiah, R. Ovsyannikov, H. A. Dürr, R. Follath, Y. Huang, S. de Jong, M. S. Golden, Yu.-Z. Zhang, H. O. Jeschke, R. Valentí, C. Felser, S. D. Farahani, M. Rotter, and D. Johrendt, *Electronic Structure Studies of* $BaFe_2As_2$ *by Angle-Resolved Photoemission Spectroscopy*, Phys. Rev. B **79**, 155118 (2009).

[31] T. Yoshida, I. Nishi, S. Ideta, A. Fujimori, M. Kubota, K. Ono, S. Kasahara, T. Shibauchi, T. Terashima, Y. Matsuda, H. Ikeda, and R. Arita, *Two-Dimensional and Three-Dimensional Fermi Surfaces of Superconducting* $BaFe_2(As_{1-x}P_x)_2$ *and Their Nesting Properties Revealed by Angle-Resolved Photoemission Spectroscopy*, Phys. Rev. Lett. **106**, 117001 (2011).

[32] H. Pfau, C. R. Rotundu, J. C. Palmstrom, S. D. Chen, M. Hashimoto, D. Lu, A. F. Kemper, I. R. Fisher, and Z. X. Shen, *Detailed Band Structure of Twinned and Detwinned* $BaFe_2As_2$ *Studied with Angle-Resolved Photoemission Spectroscopy*, Phys. Rev. B **99**, 035118 (2019).

[33] M. F. Jensen, V. Brouet, E. Papalazarou, A. Nicolaou, A. Taleb-Ibrahimi, P. Le Fèvre, F. Bertran, A. Forget, and D. Colson, *Angle-Resolved Photoemission Study of the Role of Nesting and Orbital Orderings in the Antiferromagnetic Phase of* $BaFe_2As_2$, Phys. Rev. B **84**, 014509 (2011).

[34] See Supplemental Material at http://link.aps.org/supplemental/10.1103/PhysRevX.10.041062 for a derivation of theoretical models used in this work, as well as additional resistivity measurements at zero field for $x = 0.31$ and additional magnetoresistance scaling plots.

[35] D. Hu, Z. Yin, W. Zhang, R. A. Ewings, K. Ikeuchi, M. Nakamura, B. Roessli, Y. Wei, L. Zhao, G. Chen, S. Li, H. Luo, K. Haule, G. Kotliar, and P. Dai, *Spin Excitations in Optimally P-Doped* $BaFe_2(As_{0.7}P_{0.3})_2$ *Superconductor*, Phys. Rev. B **94**, 094504 (2016).

[36] K. Matan, R. Morinaga, K. Iida, and T. J. Sato, *Anisotropic Itinerant Magnetism and Spin Fluctuations in* $BaFe_2As_2$*: A Neutron Scattering Study*, Phys. Rev. B **79**, 054526 (2009).

[37] T. Shibauchi, A. Carrington, and Y. Matsuda, *A Quantum Critical Point Lying beneath the Superconducting Dome in Iron Pnictides*, Annu. Rev. Condens. Matter Phys. **5**, 113 (2014).

[38] P. Richard, T. Sato, K. Nakayama, T. Takahashi, and H. Ding, *Fe-Based Superconductors: An Angle-Resolved Photoemission Spectroscopy Perspective*, Rep. Prog. Phys. **74**, 124512 (2011).

[39] R. Hlubina and T. M. Rice, *Resistivity as a Function of Temperature for Models with Hot Spots on the Fermi Surface*, Phys. Rev. B **51**, 9253 (1995).

[40] B. P. Stojković and D. Pines, *Theory of the Longitudinal and Hall Conductivities of the Cuprate Superconductors*, Phys. Rev. B **55**, 8576 (1997).

[41] M. Rotter, M. Tegel, D. Johrendt, I. Schellenberg, W. Hermes, and R. Pöttgen, *Spin-Density-Wave Anomaly at 140 K in the Ternary Iron Arsenide* $BaFe_2As_2$, Phys. Rev. B **78**, 020503(R) (2008).

[42] S. Ishida, T. Liang, M. Nakajima, K. Kihou, C. H. Lee, A. Iyo, H. Eisaki, T. Kakeshita, T. Kida, M. Hagiwara, Y. Tomioka, T. Ito, and S. Uchida, *Manifestations of Multiple-Carrier Charge Transport in the Magnetostructurally Ordered Phase of* $BaFe_2As_2$, Phys. Rev. B **84**, 184514 (2011).

[43] G. S. Tucker, R. M. Fernandes, D. K. Pratt, A. Thaler, N. Ni, K. Marty, A. D. Christianson, M. D. Lumsden, B. C. Sales, A. S. Sefat, S. L. Bud'Ko, P. C. Canfield, A. Kreyssig, A. I. Goldman, and R. J. McQueeney, *Crossover from Spin Waves to Diffusive Spin Excitations in Underdoped* $Ba(Fe_{1-x}Co_x)_2As_2$, Phys. Rev. B **89**, 180503(R) (2014).

[44] J. G. Analytis, J. H. Chu, R. D. McDonald, S. C. Riggs, and I. R. Fisher, *Enhanced Fermi-Surface Nesting in Superconducting* $BaFe_2(As_{1-x}P_x)_2$ *Revealed by the de Haas–van Alphen Effect*, Phys. Rev. Lett. **105**, 207004 (2010).

[45] N. V. Volkenshtein, V. P. Dyakina, and V. E. Startsev, *Scattering Mechanisms of Conduction Electrons in Transition Metals at Low Temperatures*, Phys. Status Solidi B **57**, 9 (1973).

[46] M. Eisterer, *Radiation Effects on Iron-Based Superconductors*, Supercond. Sci. Technol. **31**, 013001 (2018).

[47] X. Wang, Y. Schattner, E. Berg, and R. M. Fernandes, *Superconductivity Mediated by Quantum Critical Antiferromagnetic Fluctuations: The Rise and Fall of Hot Spots*, Phys. Rev. B **95**, 174520 (2017).

[48] H. H. Kuo, J. H. Chu, J. C. Palmstrom, S. A. Kivelson, and I. R. Fisher, *Ubiquitous Signatures of Nematic Quantum Criticality in Optimally Doped Fe-Based Superconductors*, Science **352**, 958 (2016).

[49] S. Lederer, Y. Schattner, E. Berg, and S. A. Kivelson, *Superconductivity and Non-Fermi Liquid Behavior near a Nematic Quantum Critical Point*, Proc. Natl. Acad. Sci. U.S.A. **114**, 4905 (2017).

[50] A. V. Chubukov, R. M. Fernandes, and J. Schmalian, *Origin of Nematic Order in* FeSe, Phys. Rev. B **91**, 201105(R) (2015).

[51] R. M. Fernandes, E. Abrahams, and J. Schmalian, *Anisotropic In-Plane Resistivity in the Nematic Phase of the Iron-Pnictides*, Phys. Rev. Lett. **107**, 217002 (2011).

[52] R. M. Fernandes, A. V. Chubukov, J. Knolle, I. Eremin, and J. Schmalian, *Preemptive Nematic Order, Pseudogap, and Orbital Order in the Iron Pnictides*, Phys. Rev. B **85**, 024534 (2012).

[53] S. Hosoi, K. Matsuura, K. Ishida, H. Wang, Y. Mizukami, T. Watashige, S. Kasahara, Y. Matsuda, and T. Shibauchi, *Nematic Quantum Critical Point without Magnetism in* $FeSe_{1-x}S_x$ *Superconductors*, Proc. Natl. Acad. Sci. U.S.A. **113**, 8139 (2016).

[54] A. Baum *et al.*, *Frustrated Spin Order and Strip Fluctuations in* FeSe, Commun. Phys. **2**, 14 (2019).

[55] E. Gati, A. E. Böhmer, S. L. Budko, and P. C. Canfield, *Bulk Superconductivity and Role of Fluctuations in the Iron-Based Superconductor* FeSe *at High Pressures*, Phys. Rev. Lett. **123**, 167002 (2019).

[56] A. Rosch, *Interplay of Disorder and Spin Fluctuations in the Resistivity near a Quantum Critical Point*, Phys. Rev. Lett. **82**, 4280 (1999).

[57] M. Breitkreiz, P. M. R. Brydon, and C. Timm, *Transport in Multiband Systems with Hot Spots on the Fermi Surface: Forward-Scattering Corrections*, Phys. Rev. B **89**, 245106 (2014).

[58] H. Kontani, *Anomalous Transport Phenomena in Fermi Liquids with Strong Magnetic Fluctuations*, Rep. Prog. Phys. **71**, 026501 (2008).

[59] C. H. Mousatov, E. Berg, and S. A. Hartnoll, *Theory of the Strange Metal* $Sr_3Ru_2O_7$, Proc. Natl. Acad. Sci. U.S.A. **117**, 2852 (2020).

[60] N. P. Armitage, F. Ronning, D. H. Lu, C. Kim, A. Damascelli, K. M. Shen, D. L. Feng, H. Eisaki, Z. X. Shen, P. K. Mang, N. Kaneko, M. Greven, Y. Onose, Y. Taguchi, and Y. Tokura, *Doping Dependence of an n-Type Cuprate Superconductor Investigated by Angle-Resolved Photoemission Spectroscopy*, Phys. Rev. Lett. **88**, 257001 (2002).

[61] H. Kontani, K. Kanki, and K. Ueda, *Hall Effect and Resistivity in High-*T_c *Superconductors: The Conserving Approximation*, Phys. Rev. B **59**, 14723 (1999).

[62] J. M. Harris, Y. F. Yan, P. Matl, N. P. Ong, P. W. Anderson, T. Kimura, and K. Kitazawa, *Violation of Kohler's Rule in the Normal-State Magnetoresistance of* $YBa_2Cu_3O_{7-\delta}$ *and* $(La_{1-x}Sr_x)_2CuO_4$, Phys. Rev. Lett. **75**, 1391 (1995).

[63] H. Kontani, *Theory of Magnetoresistance in Correlated Electron Systems: Modified Kohler Rule in High-*T_c *Superconductors*, Physica B (Amsterdam) **312–313**, 25 (2002).

[64] S. Kasahara, T. Shibauchi, K. Hashimoto, K. Ikada, S. Tonegawa, R. Okazaki, H. Shishido, H. Ikeda, H. Takeya, K. Hirata, T. Terashima, and Y. Matsuda, *Evolution from Non-Fermi- to Fermi-Liquid Transport via Isovalent Doping in* $BaFe_2(As_{1-x}P_x)_2$ *Superconductors*, Phys. Rev. B **81**, 184519 (2010).